Springer

KSME

Journal of Mechanical Science and Technology 29 (1) (2015) 317~323
www.springerlink.com/content/1738-494x
DOI 10.1007/s12206-014-1238-4

Reducing particle loss in a critical orifice and an aerodynamic lens for focusing aerosol particles in a wide size range of 30 nm - 10 μm †

Tae-Hyun Hwang[1], Seok-Hwan Kim[1], Soo Hyung Kim[2] and Donggeun Lee[1,*]

[1]*School of Mechanical Engineering, Pusan National University, Busan, 609-735, Korea*
[2]*Department of Nanofusion Technology, Pusan National University, Busan, 609-735, Korea*

(Manuscript Received June 1, 2014; Revised September 4, 2014; Accepted September 18, 2014)

Abstract

Most studies on particle focusing using an aerodynamic lens concentrate on loss and focusing performance of the lens itself without accounting for the critical orifice that acts as the actual inlet. If the newly proposed design for an aerodynamic lens capable of focusing particles over a wide range of 30 nm - 10 μm is integrated into the critical orifice, this will result in a huge loss of super-micron particles (> 1 μm in diameter), and the downstream aerodynamic lens will no longer have an advantage. CFD simulations were performed to investigate the loss of particles in the critical orifice and a new converging-diverging critical orifice was proposed instead of the conventional flat critical orifice to reduce the particle loss. By optimizing the angle of the converging and diverging sections as well as the relaxation chamber design, we derived an optimal design for the final aerodynamic lens and integrated system. As a result, we can generate particle beams of less than 1 mm with more than 80% penetration efficiency for particles in the 50 nm -7 μm range, and a 60% penetration efficiency for particles of 30 nm and 10 μm.

Keywords: Aerodynamic lens; Critical orifice; Converging-diverging; Relaxation chamber

1. Introduction

First proposed by Liu et al. [1, 2], an aerodynamic lens comprised of numerous orifices is a device used to generate particle beams by focusing aerosol nanoparticles at high transmission efficiency. It allows mechanical operation without any electronic control unit. Nanoparticle focusing technology using an aerodynamic lens has various applications, including efficient inlets for aerosol mass spectrometry [3-7], micro patterning and material synthesis [8-10], and biomaterial composition measuring inlets [11].

The first aerosol particle beam production was attempted using capillary tubes [12], orifices [13, 14], and contraction nozzles [15], but these methods limited focusing of particles to specific sizes. In contrast, multi-stage aerodynamic lenses comprised of 3-5 orifices with different inner diameters enables simultaneous focusing of aerosol particles over a relatively wide range at high transmission efficiency [1, 2, 16, 17]. Examples of the focusable size range of particles are Liu et al. [2]'s 25-250 nm, Zhang et al. [18]'s 60-600 nm, Wang et al. [19]'s 3~30 nm, Lee et al. [5]'s 30-300 nm and Lee et al. [20]'s 5-50 nm. These have all remained in one order of magnitude. Recently, Lee et al. [21] arranged a 7-level orifice system such that the orifice diameter decreases and then increases again. They showed that the focusable size range can be improved to two orders of magnitude, 30 nm-10 μm, by reducing the inertial impaction loss of super-micron particles with a large St. This aerodynamic lens shall be called hereafter as a wide-range aerodynamic lens.

Most existing studies have developed and evaluated aerodynamic lenses excluding the critical orifice which has been often used as a flow-limiting inlet, i.e., under the assumption that the influx of particles and gas of the aerodynamic lens is parallel to the central axis of aerodynamic lenses at a certain low pressure. In other words, gas and particle flow downstream of the critical orifice are likely simplified and might be different from the real situation. A few recent reports [22-24] of significant losses of super-micron particles at the critical orifice raised a big concern that the advantage of the wide-range aerodynamic lens will be significantly damaged if the entire aerodynamic lens system including the critical orifice is considered.

The loss of super-micron particles at the critical orifice usually occurs at the orifice surface and tube wall after the orifice, mainly due to inertial impaction and excessive focusing arising from gas accelerated to the speed of sound in the orifice body [17, 22, 23]. Meanwhile, for nanoparticles with a small

*Corresponding author. Tel.: +82 51 510 2365, Fax.: +82 51 512 5236
E-mail address: donglee@pusan.ac.kr
† Recommended by Associate Editor Suk Goo Yoon

inertia, there is diffusion loss from increased residence time often caused by the downstream vortex [23]. To reduce the diffusion loss of small particles, Wang and McMurry [17] suggested restricting the vortex through conversion of the flat (downstream) surface of the critical orifice to a conical divergent section, while Liu et al. [22] proposed a method of removing steps inside the tube-orifice assembly. However, little has been revealed about reducing or controlling the loss, even in critical orifices, for the entire range of particles including micron sizes. Most recently, only a single paper [25] succeeded to demonstrate that the critical orifice-relaxation chamber-lens assembly works properly particles between 100 nm and 3 μm in diameter. As the key idea was high-pressure operation of the aerodynamic lens system to increase aerodynamic drag, their design is optimized for Aerodyne mass spectrometer but is not for aerosol time-of-flight mass spectrometer (ATOFMS) due to the pressure mismatch. Cahill et al.'s [24] lens assembly including the critical orifice is the only design developed for the inlet of the ATOFMS. To reduce the transmission loss of super-micron particles at the critical orifice and relaxation chamber, they increased the opening of the critical orifice in an attempt to reduce the particle Stokes number by increasing the pressure and thereby relieve overfocusing or inertia impaction of particles. This idea worked for particles larger than 4 μm. However, the Stokes number of particles smaller than 3 μm becomes too small, leading to a significant divergence of particles prior to the skimmer. Since the skimmer was inevitably installed to adjust the increased pressure to the ATOFMS inlet, a significant fraction of the particles were cut off by the skimmer. Thus, it is concluded that only 4-10 μm aerosols can be delivered by their design.

As such, this study develops a novel critical orifice that is capable of effectively transmitting particles in the widest range of 30 nm-10 μm, and then integrates the wide-range aerodynamic lenses proposed by Lee et al. [21] to present a design concept for a more realistic wide-range aerodynamic lens system for the ATOFMS.

2. Numerical simulation

The critical orifice and wide-range aerodynamic lens assembly, that is, the wide-range aerodynamic lens system, was developed by checking the performance of a new type of single stage critical orifice and integrating it with the wide-range aerodynamic lens, followed by assessing the overall performance. FLUENT (version 6.2.16) was used to calculate the air flow and particle behavior inside the critical orifice and aerodynamic lens. The flow of the carrier gas was assumed as steady-state, compressible, laminar, and viscous flow, and solved by Navier-Stokes equations. The particles having various diameters were treated as spheres with the density of a standard particle (1 g/cc), and their trajectories were calculated while ignoring lift force to evaluate the size-resolved loss and focusing performance. Because of the low concentration and small diameter, the interaction between particles and influence of the particles on flow were considered negligible [5, 18, 21]. The Brownian diffusion effect was included in calculations for small particles of 30-300 nm, and the calculations were repeated five times to obtain the average values and standard deviation values in the particle beam radius and the transmission efficiency. A user defined function (UDF) was applied to reflect changes in the slip correction factor (C_c) as the gas undergoes rapid pressure changes around the neck region [19, 20]. More details are available in our previous publications [5, 20, 21].

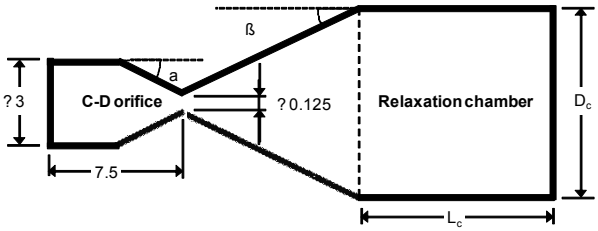

Fig. 1. Schematic of a new C-D orifice and a relaxation chamber.

For the wide-range aerodynamic lens, the inlet pressure was maintained at ~80 Pa and outlet pressure at 0.13 Pa by limiting the flux to 100 sccm (2.042 x10^{-6} kg/s) with the critical orifice having a diameter of 0.125 mm [21]. For the single-stage simulation of the critical orifice, air inflow had the same mass flow rate, and the outlet pressure was the same as the inlet pressure of the aerodynamic lens.

3. Results and discussion

3.1 Design of a new critical orifice with convergent and divergent sections

As mentioned by Chen et al. [23], the loss fraction of supermicron particles in a flat-type critical orifice can be as high as 83%, mainly at the frontal surface of and tube wall after the orifice. Wang and McMurry [17] proposed the possibility of reducing diffusion loss of small particles by modifying the relaxation chamber with a conical divergent section to reduce flow recirculation. More recently, our preceding research [20] showed that the diffusion loss of 5-50 nm particles can be significantly reduced by using a series of converging-diverging (C-D) orifices, allowing the gas flow to become shock-free and vortex-free. Thus, we decided to modify the shape of critical orifice from the conventional flat-plate orifice. Fig. 1 shows a conceptual diagram of a new C-D critical orifice we considered. The new critical orifice was divided into a C-D orifice section and a relaxation chamber, and designed for minimal particle loss in all areas. As seen in the figure, α is the converging angle, and β is the diverging angle.

3.2 C-D Orifice design: converging angle α

Even in the C-D orifice, particle loss can occur at the converging section before passing the orifice neck and at the di-

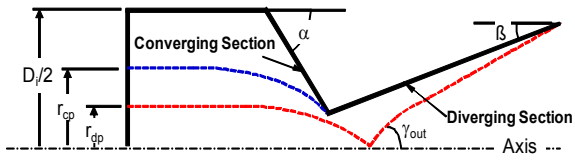

Fig. 2. Different impaction loss of particles depending on their incident radial positions.

verging section after the neck. The location where particles are lost is dependent on St number and initial radial position of particles. Fig. 2 shows two critical trajectories of super-micron particles, describing how and where the particles are lost depending on their initial radial positions. Particles are lost at the converging section if their initial radial position is greater than r_{cp}, and at the diverging section if the initial radial position is between r_{dp} and r_{cp}.

The loss fraction at the converging section (η_c) is given by Eq. (1) [15], and the loss fraction at the diverging section (η_d) is similarly expressed by Eq. (2).

$$\eta_c = \left(1 - \left(\frac{r_{cp}}{D_i/2}\right)^2\right)^2, \quad (1)$$

$$\eta_d = \left(\frac{r_{cp}^2 - r_{dp}^2}{(D_i/2)^2}\right)^2. \quad (2)$$

Fig. 3 shows the loss fraction η_c as a function of St number when the converging angle α varies between 30-90° (π/6-π/2) at a constant β = 6.2° (π/29). The angle of β was selected so as to minimize the divergent angle of particles without downstream vortex in the divergent part of the orifice (will be discussed in Sec. 3.3). For a conical diverging orifice with α = 90°, the particle loss at the converging section is almost invariant from 6% with increasing the St up to 100. When the St becomes greater than 200, there is a rapid increase in the loss at the converging section. When reducing the angle α, the curve of η_c vs St is gradually shifted to the large St direction, suggesting that the loss fraction at the converging section is gradually reduced: for α = 30° (π/6), even 10 μm particles with a St number of 1000 can be delivered with a negligible loss.

Fig. 4 gives the loss fraction η_d in terms of St number under the same conditions. Compared to Fig. 3, particles smaller than 3 μm (St < 100), after passing through the neck of the orifice with α = 90°, are lost at the diverging section, up until η_d = 45%. When the St increases more than 300, the loss fraction η_c significantly increases in Fig. 3 because of a large decrease of r_{cp} in Eq. (1), which in turn decreases the loss fraction η_d (referring to Eq. (2)).

With a decrease in α, both loss fractions decline for all values of the St. As such, the converging angle α must be minimized to prevent loss of large particles. Reducing α can prevent inertial loss of large particles, but make the critical orifice

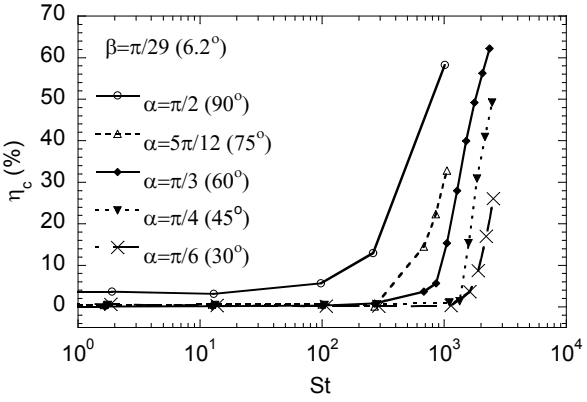

Fig. 3. St-number dependency of the fraction of particle loss at the converging section with different converging angles α.

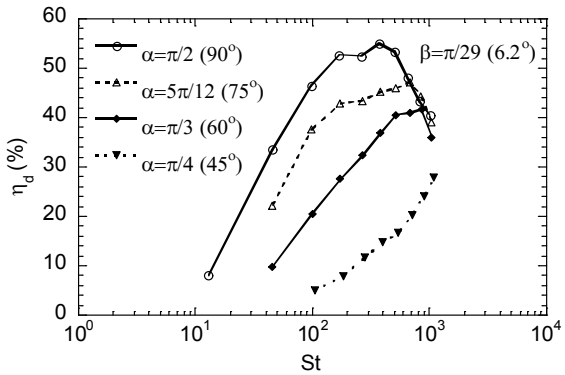

Fig. 4. St-number dependency of the fraction of particle loss at the diverging section with a fixed diverging angle β but altering the angle α.

longer. Since a longer critical orifice is expected to cause diffusion loss of small particles arising from longer residence time, the angle α was set to 30° (π/6), at which there was no loss of 10 μm particles.

3.3 C-D orifice design: Diverging angle β

In the C-D orifice, the angle β of the diverging section can affect the expanding flow of gas passing the orifice neck [20] and the diverging angle γ_{out} (refer to Fig. 2) of particles as well. As shown in Fig. 5, the diverging behavior of particles was affected differently depending on their sizes when the diverging angle β of the orifice varied over 6.2-45°. For example, for particles smaller than 300 nm, their diverging angle γ_{out} decreased with decreasing β, which was attributed to gradual decreases in the radial velocity of gas expanding at the diverging section. As seen in Fig. 6, as the β increases, the radial velocity of gas increases significantly at the diverging section, but hardly changes at the converging section. It is also a natural result that smaller particles are more affected by the expanding gas at a certain β. Thus, larger particles and a minimum β of orifice are preferred for suppressing the angle of γ_{out} in the size range of particles.

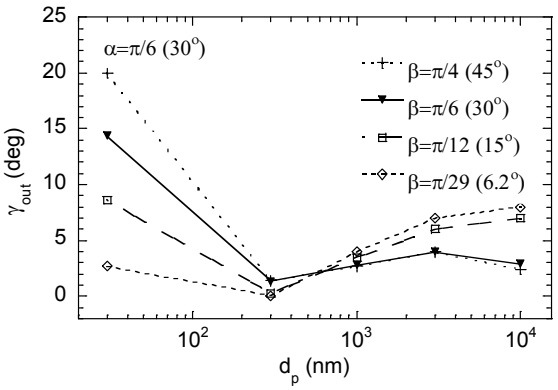

Fig. 5. Dependence of diverging angle of particles in a wide size range on their size and the angle of β.

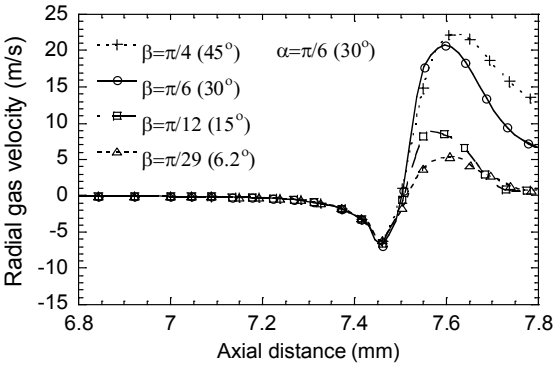

Fig. 6. Variations of radial gas velocity along the axis of the C-D nozzle with different diverging angles of β.

In contrast, the opposite was observed in Fig. 5 for particles larger than 300 nm: as β becomes smaller, the diverging angle γ_{out} of large particles increases in spite of the decrease in radial gas velocity. Unlike smaller particles, larger micron particles are hardly affected by the gas due to their greater inertia. Rather, the change in γ_{out} can be interpreted as a difference in local St numbers of micron particles right after passing through the orifice neck as follows. The local St number is defined in Eq. (3) [21].

$$St = \frac{\tau U}{D_d / 2} = \frac{\rho_p d_p^2 U C_c}{9 \eta D_d}. \quad (3)$$

In the equation, D_d is an orifice diameter at a certain spot of the diverging section, U is an average velocity of gas flow (see Fig. 10), η is the gas viscosity, and ρ_p and d_p are the density and size of particles. As seen in Fig. 7, when the angle of β is reduced from β_1 to β_2, the average gas velocity U becomes greater due to the decrease in the local diameter D_d (from $D_{d,1}$ to $D_{d,2}$). This causes an increase in the local St (greater inertia), resulting in more severe overfocusing of particles as contrasted as trajectories 1 and 2 in Fig. 7 and the increase of the γ_{out} as well.

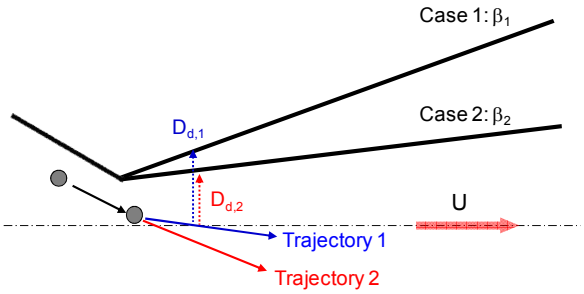

Fig. 7. Effect of diverging angle β on particle trajectories: difference in local St number at the diverging section.

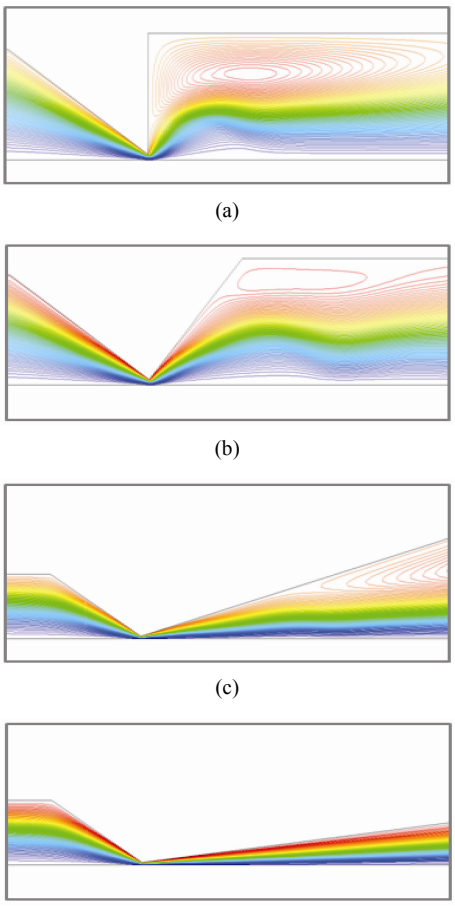

Fig. 8. Gas streamlines in the C-D critical orifices with different diverging angles: (a) β = π/2; (b) β = π/4; (c) β = π/12; (d) β = π/29.

In the C-D orifice, reducing the diverging angle γ_{out} of large particles helps to shorten the relaxation chamber that connects to the rear side of the C-D orifice. However, for $\beta \leq 30^o$ (π/12), the diverging angle of micron particles does not show significant differences even with a further decrease in β, and thus has no effect on the design of the relaxation chamber. As mentioned before, when β increases, gas flow becomes unstable due to the formation of a vortex near the diverging section, and the back flow and recirculation result in a greater loss of

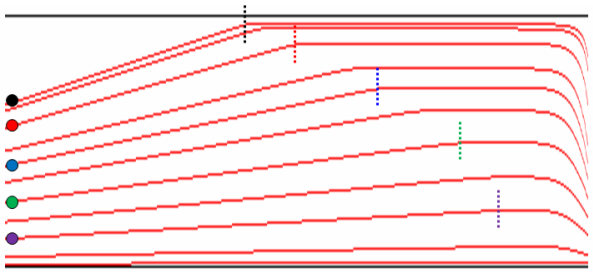

Fig. 9. Different trajectories of particles entering the relaxation chamber at different radial positions: the bending points denoted by a dotted short line are shifted downstream as the incident radial position of particles gets closer to the axis.

small particles [23]. As shown in Fig. 8, the β was set as 6.2° (π/29) to prevent the vortex formation.

3.4 Relaxation chamber design

Since particles flowing out of the CD orifice at the diverging angle γ_{out} can undergo additional loss at the wall of relaxation chamber, an adequate diameter (D_c) and length (L_c) must be selected for the relaxation chamber shown in Fig. 1. In the relaxation chamber, the redeveloped flow line is parallel to the horizontal axis, resulting in zero radial velocity of gas. Here, particles entering the relaxation chamber with the diverging angle γ_{out} are gradually decelerated to the radial direction by the drag force F_D and eventually move horizontally after a relaxation time τ. The radial stopping distance (S_y) particles travel until the horizontal movement is estimated by multiplying the size-dependent τ by the radial velocity component ($V_{p,y}$) of particles at the inlet of the relaxation chamber. Hence, the S_y is affected by the initial speed, diverging angle, and size of entering particles. The loss of large particles at the relaxation chamber can be minimized by designing the inner diameter D_c of the relaxation chamber to be larger than the maximum S_y.

Consider the situation in which particles enter the relaxation chamber at different radial positions: near and far from the axis. As the incidence position of particles gets closer to the axis, the radial velocity of particles declines and their axial velocity increases instead, allowing the particles travel a longer axial distance until their trajectory becomes parallel to the axis. As confirmed in Fig. 9, the bending point of the trajectories is gradually shifted downstream when the incidence position of particles gets closer to the axis. The minimum length of the relaxation chamber (denoted as L_c) was designed to be slightly larger than the longest axial distance to the bending point.

3.5 Performance evaluation of the aerodynamic lens system

As stated earlier, the final critical orifice was integrated with the existing wide-range aerodynamic lens to form an aerodynamic lens (ADL) system. Fig. 10 shows the trajectories of particles with various sizes in the ADL system. Even for the entire ADL system, all particles of interest could be effectively focused regardless of their size. The trajectories of particles of 30 nm or even 300 nm show a discernible Brownian effect when comparing the cases of with and without Brownian effect.

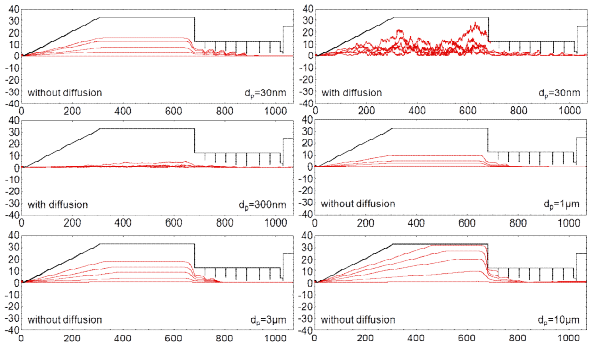

Fig. 10. Trajectories of particles with various diameters in an Aerodynamic lens system; all values in the x and y axes are in units of millimeters and the x and y scales are different.

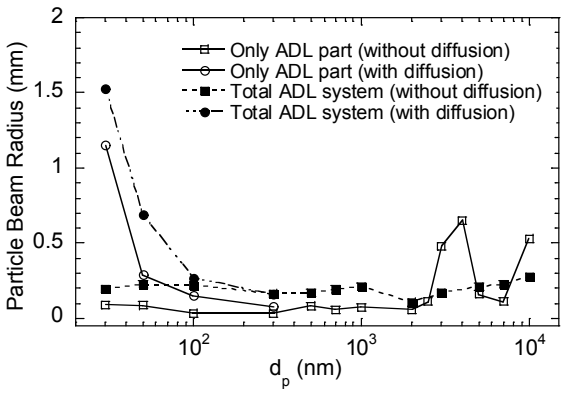

Fig. 11. Comparisons of radii of particle beams focused by the aerodynamic lens only and the entire ADL system when the diffusion effect is included or not.

Fig. 11 presents the beam radius of particles focused via the ADL system against their size in consideration of 90% flux (enclosing 90% of the total particle flux) 40 mm downstream the exit of the final nozzle of the ADL system. This was compared with results for the aerodynamic lens, only excluding the critical orifice. When diffusion of sub-micron particles is taken into account, the average beam radius was found to 1.55 mm for 30 nm, and 0.75 mm for 50 nm. Even for 100 nm, there is a considerable Brownian effect degrading the focusing performance. This strengthened Brownian effect is mainly due to the longer residence time of particles passing the lengthened ADL system. Over the 100 nm - 10 μm range, the beam radius of 0.3 mm was slightly larger than the value derived only for the aerodynamic lens, but still effective in focusing particles.

Likewise, Fig. 12 shows the transmission efficiency of the ADL system by particle size along with the existing results for

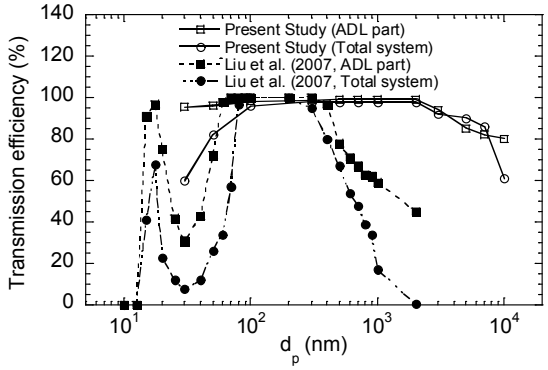

Fig. 12. Comparisons of transmission efficiencies of particles between the present C-D type ADL system and Liu et al.'s one.

the aerodynamic lens only [21]. These results were also compared with the results obtained by Liu et al. [22]. From 100 nm to 3 μm, the critical orifice is clearly an effective inlet as it has a high transmission efficiency of 92%. For smaller particles of 50 nm and 30 nm, the diffusion loss at the relaxation chamber leads to a lower but still acceptable transmission efficiency of 84% and 60%, respectively. For 10 μm particles, the transmission efficiency was 60% due to inertial impaction loss at the critical office. In summary, we have proposed a novel design of converging-diverging critical orifice and relaxation chamber assembly in an attempt to reduce the particle loss arising from inertial impaction and diffusion. We also proved the possibility of effectively focusing particles over a wide range of 30 nm – 10 μm through integration with the existing ADL system.

Finally, there are some technological limitations for the final design of the critical orifice-relaxation chamber-ADL assembly. One of the limitations is that the proposed critical orifice with a 6 degree included angle might be a bit of a challenge to manufacture, especially with a conventional tool such as drilling and tapering. However, recent progress in manufacturing technology, including rapid prototyping and sheet metals, allows to manufacture the C-D orifice with 10 degree or less in the very near future. Second, the flow Reynolds number through the critical orifice is ~1140, suggesting the possibility that the flow is not necessarily laminar. Here, it is worth noting that other ADL systems including a thin-plate critical orifice with a similar size (denoting a similar Re number) were demonstrated experimentally to work properly [3, 5, 22]. In addition, because the C-D type of orifice can stabilize downstream gas flow better than the thin-plate orifice [20], the turbulence issue might be possibly ruled out. However, it is also true that experimental works for the C-D type orifice are very limited to demonstrate that the orifice turbulence is not an issue.

4. Conclusions

We have designed a new converging-diverging type critical orifice and a relaxation chamber as an efficient inlet enabling to minimize transmission loss of particles in a wide size range of 30 nm - 10 μm. Key ideas in design of the C-D critical orifice are 1) to minimize the converging angle α of the C-D orifice as long as it does not cause a significant diffusion loss of particles, leading to a great reduction in impaction loss of large particles, and 2) to minimize the diverging angle β for reducing the diverging angle γ_{out} of particles and preventing the flow recirculation at the diverging section. The relaxation chamber was designed to enlarge its diameter over the maximal stopping distance of particles to the radial direction and to be long enough for allowing all particle trajectories to become parallel to the axis. After integration with the wide-range aerodynamic lens developed in past research, the entire aerodynamic lens system was confirmed to produce particle beams with radii smaller than 1 mm with a relatively high transmission efficiency: 60% of 30 nm and 10 μm particles and > 80% for 50 nm - 7 μm particles.

Acknowledgment

This work was supported by the National Research Foundation of Korea (NRF) grant funded by the Korea Government (MSIP) (No. NRF-2010-0019543), by PM2.5 research center supported by MSIP and National Research Foundation of Korea (No. NRF-2014M3C8A5030614), and also by the Global Frontier R&D Program on Center for Multiscale Energy System funded by the National Research Foundation under the MSIP (No. NRF-2012M3A6A7054863).

References

[1] P. Liu, P. Ziemann, D. Kittelson and P. McMurry, Generation of particle beams of controlled dimensions and divergence: I. Theory of particle motion in aerodynamic lenses and orifice expansions, *Aerosol Sci. Technol.*, 22 (1995) 293-313.

[2] P. Liu, P. Ziemann, D. Kittelson and P. McMurry, Generation of particle beams of controlled dimensions and divergence: II. Experimental evaluation of particle motion in aerodynamic lenses and orifice expansions, *Aerosol Sci. Technol.*, 22 (1995) 314-324.

[3] D. Lee, K. Park and M. Zachariah, Determination of size distribution of polydisperse nanoparticles with single particle mass spectrometry: The role of ion kinetic energy, *Aerosol Sci. Technol.*, 39 (2005) 162-169.

[4] D. Lee, A. Miller, D. Kittelson and M. Zachariah, Characterization of metal-bearing diesel nanoparticles using single particle mass spectrometry, *J. Aerosol Sci.*, 37 (1) (2006) 88-110.

[5] K. Lee, S. Cho and D. Lee, Development and experimental evaluation of aerodynamic lens as an aerosol inlet of single mass spectrometry, *J. Aerosol Sci.*, 39 (2008) 287-304.

[6] Y. Su, M. F. Sipin, H. Furutani and K. A. Prather, Development and characterization of an aerosol time-of-flight mass

spectrometer with increased detection efficiency, *Anal. Chem.*, 76 (2004) 712-719.

[7] D. Y. Liu, D. Rutherford, M. Kinsey and K. A. Prather, Real-time monitoring of pyrotechnically derived aerosol particles in the troposphere, *Anal. Chem.*, 69 (10) (1997) 1808-1814.

[8] Y. Dong, A. Bapat, S. Hilchie, U. Kortshagen and S. Campbell, Generation of nano-sized free standing single crystal silicon particles, *J. Vac. Sci. Technol. B*, 22 (4) (2004)1923-1930.

[9] F. Fonzo, A. Gidwani, M. Fan, D. Neumann, D. Iordanoglou, J. Heberlein, P. McMurry, S. Girshick, N. Tymiak, W. Gerberich and N. Rao, Focused nanoparticle-beam deposition of patterned microstructures, *Appl. Phys. Lett.*, 77 (6) (2000) 910-912.

[10] L. Qi, P. MuMurry, D. Norris and S. Girshick, Micropattern deposition of colloidal semiconductor nanocrystals by aerodynamic focusing, *Aerosol Sci. Technol.*, 44 (2010) 55-60.

[11] W. Harris, P. Reilly and W. Whitten, Aerosol MALDI of peptides and proteins in an ion trap mass spectrometer: Trapping, resolution and signal-to-noise, *Int. J. Mass. Spectrom*, 258 (2006) 113-119.

[12] W. Murphy and G. Sears, Production of particulate beams, *J. Appl. Phys.*, 35 (1964) 1986-1987.

[13] R. Das and D. Phares, Expansion of an ultrafine aerosol through a thin-plate orifice, *J. Aerosol Sci.*, 35 (2004) 1091-1103.

[14] R. Deng, X. Zhang, K. Smith, J. Wormhoudt, D. Lewis and A. Freedman, Focusing particle with diameters of 1 to 10 microns into beams at atmospheric pressure, *Aerosol Sci. Technol.*, 42 (2008) 899-915.

[15] D. Chen and Y. Pui, Numerical and experimental studies of particle deposition in a tube with a conical contraction-laminar flow regime, *J. Aerosol Sci.*, 26 (4) (1995) 563-574.

[16] X. Wang and P. McMurry, An experimental study of nanoparticle focusing with aerodynamic lenses, *Int. J. Mass. Spectrom*, 258 (2006) 30-36.

[17] X. Wang and P. McMurry, A design tool for aerodynamic lens systems, *Aerosol Sci. Technol.*, 40 (2006) 320-334.

[18] X. Zhang, K. Smith, D. Worsnop, J. Jimenez, J. Jayne, C. Kolb, J. Morris and P. Davidovits, Numerical characterization of particle beam collimation: Part II Integrated aerodynamic-lens-orifice system, *Aerosol Sci. Technol.*, 38 (2004) 19-638.

[19] X. Wang, A. Gidwani, S. Girshick and P. McMury, Aerodynamic focusing of nanoparticles: II. Numerical simulation of particle motion through aerodynamic lenses, *Aerosol Sci. Technol.*, 39 (2005) 624-636.

[20] K. Lee, S. Kim and D. Lee, Aerodynamic focusing of 5-50 nm nanoparticles in air, *J. Aerosol Sci.*, 40 (2009) 1010-1018.

[21] K. Lee, T. Hwang and D. Lee, A numerical analysis of the aerodynamic focusing of particles with wide-range diameters of 30 nm-10 μm, *Aerosol Sci. Technol.*, 47 (2013) 1001-1008.

[22] P. Liu, R. Deng, K. Smith, L. Williams, J. Jayne, M. Canagaratna, K. Moore, T. Onasch, D. Worsnop and T. Deshler, Transmission efficiency of an aerodynamic focusing lens system: Comparison of model calculations and laboratory measurements for the aerodyne aerosol mass spectrometer, *Aerosol Sci. Technol.*, 41 (2007) 721-733.

[23] S. Chen, C. Tsai, C. Wu, D. Pui, A. Onischuk and V. Karasev, Particle loss in a critical orifice, *J. Aerosol Sci.*, 38 (2007) 935-949.

[24] J. F. Cahill, T. K. Darlington, X. Wang, J. Mayer, M. T. Spencer, J. C. Holecek, B. E. Reed and K. A. Prather, Development of a high-pressure aerodynamic lens for focusing large particles (4-10 μm) into the aerosol time-of-flight mass spectrometer, *Aerosol Sci. Technol.*, 48 (9) (2014) 948-956.

[25] L. R. Williams et al., Characterization of an aerodynamic lens for transmitting particles greater than 1 micrometer in diameter into the aerodyne aerosol mass spectrometer, *Atmos Meas. Tech.*, 6 (2013) 3271-3280.

Donggeun Lee is a Professor at School of Mechanical Engineering, Pusan National University and is now leading a basic research lab (BRL) and a Nanoparticle engineering lab. More information is available in http://home.pusan.ac.kr/~mnht.